ADVANCED HEALTHCARE MATERIALS
www.advhealthmat.de

A Pseudo-Surfactant Chemical Permeation Enhancer to Treat Otitis Media via Sustained Transtympanic Delivery of Antibiotics

Sophie S. Liu, Joanna M. White, Zhongmou Chao, Ruye Li, Shuxian Wen, Ally Garza, Wenjing Tang, Xiaojing Ma, Pengyu Chen, Susan Daniel, Frank S. Bates, Jingjie Yeo, Michelle A. Calabrese, and Rong Yang**

Chemical permeation enhancers (CPEs) represent a prevalent and safe strategy to enable noninvasive drug delivery across skin-like biological barriers such as the tympanic membrane (TM). While most existing CPEs interact strongly with the lipid bilayers in the stratum corneum to create defects as diffusion paths, their interactions with the delivery system, such as polymers forming a hydrogel, can compromise gelation, formulation stability, and drug diffusion. To overcome this challenge, differing interactions between CPEs and the hydrogel system are explored, especially those with sodium dodecyl sulfate (SDS), an ionic surfactant and a common CPE, and those with methyl laurate (ML), a nonionic counterpart with a similar length alkyl chain. Notably, the use of ML effectively decouples permeation enhancement from gelation, enabling sustained delivery across TMs to treat acute otitis media (AOM), which is not possible with the use of SDS. Ciprofloxacin and ML are shown to form a pseudo-surfactant that significantly boosts transtympanic permeation. The middle ear ciprofloxacin concentration is increased by 70-fold in vivo in a chinchilla AOM model, yielding superior efficacy and biocompatibility than the previous highest-performing formulation. Beyond improved efficacy and biocompatibility, this single-CPE formulation significantly accelerates its progression toward clinical deployment.

1. Introduction

Chemical permeation enhancers (CPEs) are molecules commonly used to enable the delivery of therapeutics across biological barriers. To date, over 600 CPEs have been discovered – and many approved by the Food and Drug Administration (FDA) – to improve the permeability of epithelial membranes for drug delivery.[1] The existing CPEs span a variety of molecular chemistries and are broadly categorized into solvents, surfactants, terpenes, azones, fatty acids, urea, phospholipids, etc.[2] For skin penetration, CPEs predominantly act on the intercellular lipid matrix, disrupting the tightly packed crystalline lipid lamellae and creating defects to enable the permeation of therapeutics.[3]

Despite the variety of existing CPEs, new molecular design strategies are required to meet the evolving needs in drug delivery across biological barriers. For example, to achieve sustained barrier-crossing capability and ease of delivery, CPEs and therapeutics are often codelivered in a

S. S. Liu, Z. Chao, S. Wen, W. Tang, X. Ma, P. Chen, S. Daniel, R. Yang
Robert F. Smith School of Chemical and Biomolecular Engineering
Cornell University
Olin Hall, Ithaca, NY 14850, USA
E-mail: ryang@cornell.edu

S. S. Liu
Meinig School of Biomedical Engineering
Cornell University
Weill Hall, Ithaca, NY 14850, USA

J. M. White, F. S. Bates, M. A. Calabrese
Department of Chemical Engineering and Materials Science
University of Minnesota
421 Washington Ave., Minneapolis, MN 55455, USA
E-mail: mcalab@umn.edu

R. Li
Department of Chemistry and Chemical Biology
Cornell University
Baker Laboratory, Ithaca, NY 14850, USA

A. Garza
Department of Health and Biomedical Sciences
University of Texas Rio Grande Valley 1201 W University Drive
Edinburg, TX 78539, USA

J. Yeo
Sibley School of Mechanical and Aerospace Engineering
Cornell University
Upson Hall, Ithaca, NY 14850, USA

The ORCID identification number(s) for the author(s) of this article can be found under https://doi.org/10.1002/adhm.202400457

DOI: 10.1002/adhm.202400457

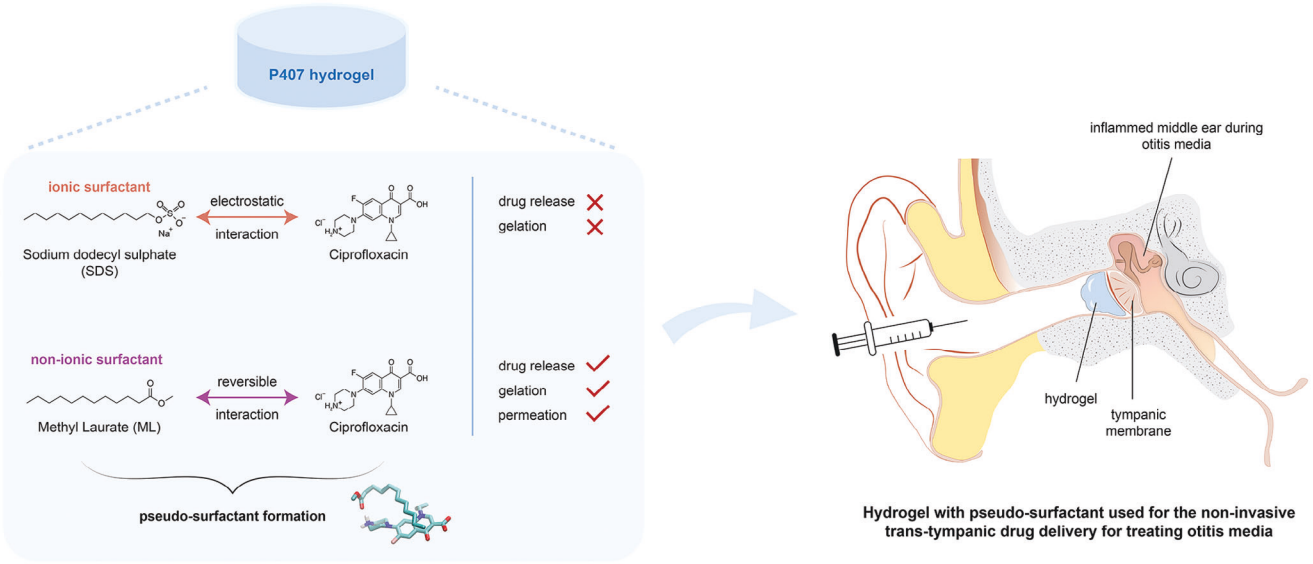

Figure 1. Schematic illustration of the hydrogel formulations used in this study. The formulations contain a temperature-responsive hydrogel, poloxamer 407 (P407), a broad-spectrum antibiotic, ciprofloxacin, and different chemical permeation enhancers (CPEs), including methyl laurate (ML), for the local, noninvasive treatment of acute otitis media (AOM).

temperature-responsive hydrogel, such as one made of poloxamer 407 (P407) – a triblock polymer which can gel in aqueous solutions near body temperature. However, certain CPEs, such as the ionic surfactant sodium dodecyl sulfate (SDS), are known to interfere strongly with the micellization of P407, inhibiting gelation.[4] Ionic surfactants can also interact strongly with therapeutics (e.g., ionic interactions between SDS and the antibiotic drug ciprofloxacin),[5] resulting in the formation of aggregates with slow diffusion through the hydrogel.[6] As ionic surfactants make up a large class of commonly used transdermal CPEs,[1,2] the CPE-drug-hydrogel interactions present a significant formulation challenge, constraining the development of hydrogel-based drug delivery systems for barrier crossing. While that challenge could be addressed by designing new polymer chemistries or structures,[7] new compounds may also come with prolonged approvals and considerable uncertainties during the translation to clinical practice.

Herein, we report a fresh strategy of harnessing drug-excipient interactions to form a "pseudo-surfactant" in hydrogel formulation, which effectively enhances tissue penetration without disrupting the reverse thermal gelation of the overall formulation. We illustrate this strategy using methyl laurate (ML), a polar but nonionic fatty acid ester with a similar C_{12} aliphatic chain as SDS. Using experimental and computational techniques simultaneously, we show that ML and the antibiotic ciprofloxacin interact synergistically in a P407-rich environment, reversibly forming a complex we termed as a "pseudo-surfactant", enhancing tissue permeability while retaining the structure and rheological behavior of a P407 hydrogel.

We highlight the benefits of this fresh strategy by using such a formulation to overcome the biological barrier of the tympanic membrane (TM) in the context of treating acute otitis media (AOM, i.e., middle ear infection), one of the most common pediatric conditions affecting over two-thirds of U.S. children.[8] The delivery of antibiotics directly to the middle ear is much preferred compared to the current standard of care, i.e., a multiday course of oral antibiotics.[8] The systemic exposure of antibiotic could lead to acute side effects[9] in children and risks of antibiotic resistance (e.g., from failure to adhere to the prescribed regimes or frequent antibiotic usage to treat recurrent AOM episodes).[10] However, the local treatment requires that the TM, one of the most impermeable biological barriers, be overcome to deliver antibiotics directly to the middle ear. Similar to the skin, the TM comprises a stratum corneum layer with a brick-and-mortar structure, making it impenetrable to most drugs[11] This impermeability is why most FDA-approved ciprofloxacin-containing ear drops, e.g., Ciprodex[12] and Cetraxal,[13] are only approved for use in children with perforated TM.

Using the fresh strategy of pseudo-surfactants, we leverage FDA-approved compounds to decouple gelation and permeation enhancement via designed excipient-drug-hydrogel interactions (**Figure 1**). This formulation significantly boosts antibiotic permeation in an in vitro model of supported lipid bilayers (SLB) and an ex vivo model using healthy and intact chinchilla TMs. Similar permeation enhancement cannot be achieved using ML or ciprofloxacin alone. Moreover, the temperature-induced gelation of P407 is preserved after adding ML – unlike the commonly used ionic surfactant SDS which prevents P407 gelation. The retained gelation enables a convenient single-dose administration of a liquid formulation through the outer ear canal, which subsequently gels to hold the formulation near the TM and enables sustained delivery over seven days. Its efficacy is superior to a combination of three CPEs (1% w/v SDS, 2% w/v limonene, and 0.5% w/v bupivacaine, termed "3CPE(SDS)") previously identified as best-in-class for hydrogel-based transtympanic drug delivery.[7,14]

Although ML and other fatty acid methyl esters (FAMEs) are considered CPEs in transdermal drug delivery,[1a,15] we emphasize that ML does not act as a CPE alone here; instead, ML and ciprofloxacin are both required to achieve permeation enhancement. This is explored by measuring the electrochemical

impedance of supported lipid bilayers as a proxy of the lipid bilayers' permeability in the TM stratum corneum. Furthermore, it is shown that the pseudo-surfactant does not form in the absence of P407, highlighting the importance of the designed environment to enable the reported strategy; that environment was absent in most existing reports on the permeation enhancement of ML. As such, the pseudo-surfactant reported here represents an unprecedented strategy. The underlying principles are systematically unravelled using rigorous structure studies, experimentally via small-angle X-ray scattering (SAXS) and computationally using density functional theory (DFT) calculations. The fresh concept of a pseudo-surfactant CPE has the potential to significantly expand the design space for CPEs while adhering to the FDA-approved compound database, thus accelerating the progression along the discovery-to-deployment continuum.

2. Results

2.1. ML Retained the Assembly and Gelation of P407 Hydrogel and Maintained a High Rate of Drug Release from the Hydrogel

The effect of ML on the structure and thermodynamics of P407 gelation was first investigated through rheology, differential scanning calorimetry (DSC), and SAXS, and compared to that of the anionic surfactant SDS. While P407 micellization and gelation processes have been extensively reported,[16] careful characterization at this specific concentration was necessary to serve as a comparison point for formulations containing CPEs.

P407 is an ABA triblock polymer composed of poly(ethylene oxide) (PEO) endblocks and a poly(propylene oxide) (PPO) midblock. With increasing temperature, the interactions between water and the PPO midblock (and, to a lesser extent, the PEO endblocks) become less favorable, driving the formation of spherical micelles composed of PPO cores and PEO coronas.[16] When a critical volume fraction of micelles is achieved, the micelles order into cubic packings, causing the low-viscosity solutions to gel.[16a,17]

In an aqueous solution of 18% w/v P407, i.e., [P407], we captured the micellization transition using DSC, with PPO dehydration and micellization corresponding to a broad endothermic peak in the heat flow trace (Figure S1a, Supporting Information).[16a,d,17b,18] Micelle formation was also apparent in the 1D SAXS trace at 25 °C (Figure S1b, black, Supporting Information), evidenced by the broad peak at approximately $q = 0.035$ Å^{-1}; $q = 4\pi\lambda^{-1}\sin(\theta/2)$ is the magnitude of the scattering wave vector, where λ is the radiation wavelength and θ is the scattering angle. Consistent with prior reports,[19] further temperature increases resulted in a many-order-of-magnitude increase in the dynamic moduli as the formulations underwent the solution-to-gel transition (Figure S1a, Supporting Information). This transition, occurring at ≈27 °C, corresponds to the micelles ordering into a face-centered cubic (FCC) packing, as evidenced by the appearance of sharp Bragg peaks in the SAXS traces at characteristic positions of $q/q^* = 1$, $\sqrt{(4/3)}$, $\sqrt{(8/3)}$, $\sqrt{(11/3)}$, 2 which correspond to the (111), (200), (220), (311), and (222) crystallographic planes (Figure S1b, Supporting Information).[19c,20] The radius of the micelles, R_{mic}, was estimated as half of the nearest-neighbor distance between micelles on the FCC lattice. For [P407], R_{mic} = 109 Å at 35 °C. This micelle size closely matched the hydrodynamic radius, R_h, of micelles in a 1% w/v P407 solution at 37 °C measured by dynamic light scattering (DLS) (**Figure 2d**) and is consistent with P407 micelle sizes reported previously.[16a,f,21]

Consistent with prior reports,[4c,22] the addition of 2% w/v SDS to an 18% w/v P407 solution, i.e., [P407 + 2% SDS], eliminated gelation, resulting in a low-modulus liquid across the examined temperature range (Figure 2a). This disruption to gelation, observed for a range of P407 and SDS concentrations, stems from SDS-P407 interactions that impede temperature-dependent micellization.[4c,22c] Here, the absence of P407 micellization was confirmed via DSC and SAXS, consistent with prior reports indicating that P407 micellization can be inhibited entirely above a critical SDS concentration (>2×10^{-3} M SDS in an aqueous solution containing 1% w/w P407).[4c,22e] In the DSC trace (Figure 2b), no endothermic peak was present for [P407 + 2% SDS], and its SAXS trace at 35 °C (near body temperature) had no distinguishable features (Figure 2c). To probe the structure of P407/SDS solutions further, DLS was performed on solutions of 1% w/v P407 with 0.1% w/v SDS (approximately a tenfold dilution from [P407 + 2% SDS]), revealing a highly dispersed population of aggregates with an average R_h of 47 Å (Figure 2d; Figure S2.1, Supporting Information). This size is consistent with that of an SDS micelle stabilized by a single P407 chain (Figure 2e), as observed previously.[22c] Thus, as P407 micellization is a critical precursor to gelation, the addition of SDS prevented the solution-to-gel transition of the P407 formulation by disrupting P407 micellization.

Unlike SDS, which is readily soluble in water, ML has a very low aqueous solubility (<0.008 g L^{-1} at 25 °C). The addition of P407 (18% w/v) to aqueous solutions of 2% w/v ML, i.e., [P407 + 2% ML], appeared to stabilize ML droplets, forming a uniformly semicloudy emulsion (Figure 2f). The resulting gels were imaged via optical microscopy at 37 °C. These images showed clear ML droplets with a droplet diameter on the order of 10 µm (Figure 2f). Interestingly, [P407 + 2% ML] demonstrated similar gelation and micelle-assembly behavior as [P407]. Rheology and DSC showed that ML addition only slightly decreased the micellization and gelation temperatures (Figure 2a,b; Figure S3, Supporting Information), and SAXS confirmed that the gel at 35 °C contained FCC-packed micelles with virtually identical size to that of [P407] (Figure 2c). To supplement the aforementioned measurements that were performed on concentrated formulations, DLS and SAXS were performed on dilute solutions of 1% w/v P407 with 0.1% w/v ML (matching that of the DLS measurements performed on [P407 + SDS]) (Figure 2d; Figure S2.1, Supporting Information) for DLS and 2.5% w/v P407 with 2% w/v ML for SAXS (Figure S4, Supporting Information). Consistent with the SAXS results at higher concentration, the hydrodynamic radius and micelle radius in dilute solutions was nearly identical to that of P407 without ML, suggesting negligible ML incorporation into the P407 micelles.

Drug diffusion through the hydrogel was examined via in vitro release studies using a Transwell membrane under infinite sink conditions. Test formulations contained 18% w/v P407, 4% w/v ciprofloxacin, and various CPEs. Unsurprisingly, the cumulative drug release at 120 hours was lowered by the presence of 18% w/v P407, with 73.5 ± 3.5% release achieved by [P407 + cip] compared to 95.6 ± 6.7% achieved by [cip in H_2O] (Figure S5.1, Supporting

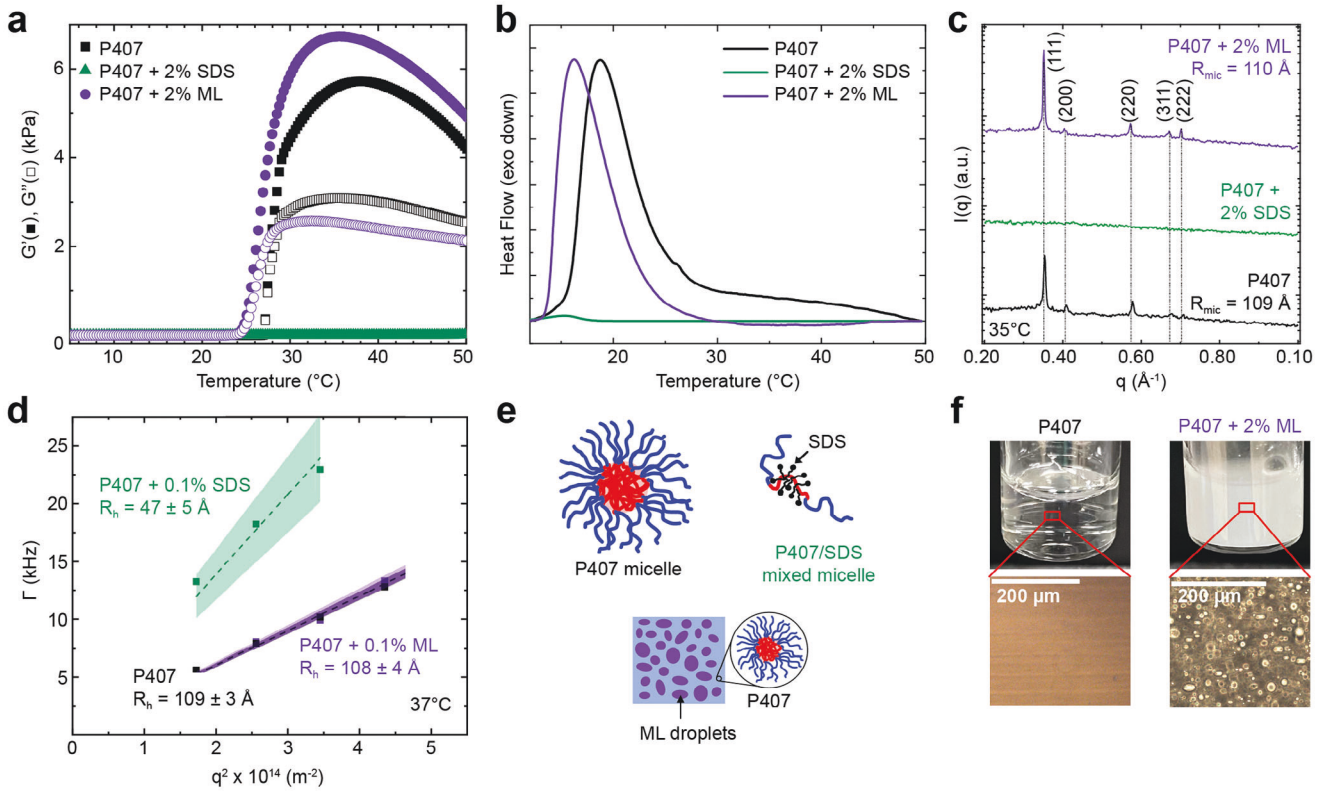

Figure 2. Micelle formation and gelation for P407 solutions with SDS and ML. a) Rheology data showing the absence of a temperature-dependent rheological transition in 18% w/v P407 with 2% w/v SDS, while the addition of 2% w/v ML to the 18% w/v P407 maintained the solution-to-gel transition. b) DSC data showing the absence of the temperature-dependent thermodynamic micellization transition in 18% w/v P407 with 2% w/v SDS, while 2% w/v ML preserved that micellization. c) 1D SAXS data at 35 °C illustrating the absence of a well-defined or ordered population of micelles for 18% w/v P407 with 2% w/v SDS, while the addition of 2% w/v ML preserved the gel structure of FCC-packed micelles seen in 18% w/v P407. Peaks were labeled with the corresponding lattice planes. d) Decay coefficient (Γ) determined via multiangle Dynamic Light Scattering (DLS), plotted as a function of q^2 for 1% w/v P407 solutions with 0.1% w/v ML or SDS. Error bands represent the 95% confidence interval around the slope. The R_h values are determined from the Stokes–Einstein equation and are reported as the mean ± 95% confidence interval. See Section S2 in the Supporting Information for further information. e) Schematics (not to scale) of solutions of P407, P407 + SDS mixture, and P407 + ML mixture. As suggested by Kancharla et al.,[22c] the SDS-containing solutions formed mixed micelles of SDS stabilized by a P407 chain; whereas ML likely formed micron-sized oil droplets that were minimally incorporated into the P407 micelles. f) Optical image and micrographs of clear gels of 18% w/v P407 and cloudy gels of 18% w/v P407 with 2% w/v ML at 37 °C. Optical microscope images reveal the micron-sized oil droplets formed by ML. Scale bar = 200 µm.

Information). Adding 2% w/v ML, i.e., [P407 + cip + 2% ML], had a negligible effect on drug elution, leading to a cumulative release of 69.5 ± 3.4%, similar to that of [P407 + cip] (Figure S5.2, Supporting Information).

On the contrary, 1% SDS drastically reduced the hydrogel drug release in [P407 + cip + 1% SDS] to 36.6 ± 2.5% ciprofloxacin at 120 h ($p < 0.001$ vs [P407 + cip]), and 2% SDS was able to reduce that even further (Figure S5.1, Supporting Information). This reduction was likely caused by the insoluble aggregates (Figure S5.3, Supporting Information) formed between the drug and SDS via electrostatic interactions among the sulfate group (in SDS) and the amine group (in ciprofloxacin).[6] This also likely contributed to the drug release reduction for 3CPE(SDS) to 51.0 ± 3.5% ($p < 0.01$ versus [P407 + cip]) (Figure S5.1, Supporting Information), consistent with previous observations.[7] The 3CPE(SDS) is the best-in-class transtympanic CPE combination, and it contained 1% SDS, along with 0.5% bupivacaine and 2% limonene[7]

2.2. ML and Ciprofloxacin Interacted to form a Pseudo-Surfactant within the P407 Hydrogel

Molecular dynamics (MD) simulations probing ciprofloxacin and ML interactions within a P407 micelle supported the formation of pseudo-surfactant, with ciprofloxacin and the ester group of ML serving as a hydrophilic headgroup and the ML hydrocarbon chain imparting lipophilicity within the tail (**Figure 3a**). Within the confines of the P407 micellar domain, ciprofloxacin and ML consistently exhibited an affinity for association, evidenced by a persistent center of mass (COM) distance between ciprofloxacin and ML that was less than 6 Å (Figure 3a; Figure S6.1, Supporting Information). In contrast, in aqueous solution, ciprofloxacin and ML predominantly dissociated, as the COM distance typically surpassed 10 Å (Figures S6.1 and S6.2, Supporting Information), which was also congruent with experimental observation for the phase separation between ciprofloxacin and ML in aqueous environment (Figure S7, Supporting Information).

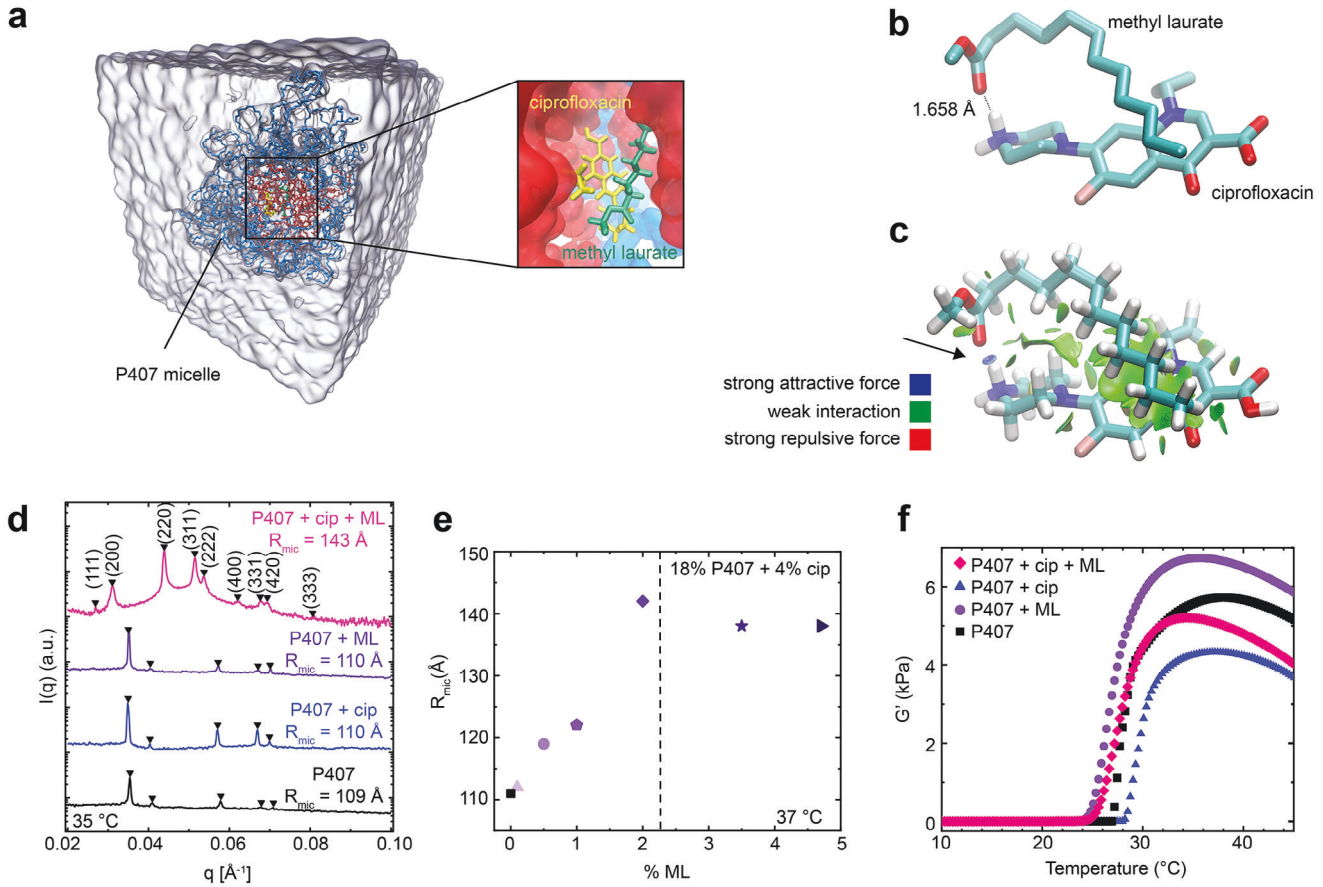

Figure 3. Characterization of hydrogel formulations illustrating pseudo-surfactant formation. a) Molecular dynamics (MD) simulation of the P407 self-assembly into micelles in water, with poly(ethylene glycol) blocks shown in blue and poly(propylene glycol) blocks shown in red. The water solvent is shown as translucent surface. Inset: possible micellar conformations of ML and ciprofloxacin, shown in green and yellow respectively, that were extracted from the MD simulations for further analysis in [b] and [c]. b) Illustration of the complexation between ML and ciprofloxacin predicted from density functional theory (DFT) calculation. Hydrogens not involved in hydrogen-bonding have been omitted for clarity. c) Noncovalent interaction (NCI) analysis reveals a hydrogen bonding (black arrow) between ML's carbonyl group and ciprofloxacin's secondary amine group, and π-alkyl interactions between ML's alkyl chain and ciprofloxacin's quinolone ring. d) SAXS traces at 35 °C showing unchanged micelle radius, R_{mic}, with the addition of either 4% w/v ciprofloxacin or 2% w/v ML to an 18% w/v P407 solution, whereas the addition of both increased the lattice size and the corresponding R_{mic}. All formulations formed an FCC lattice, as indicated by black triangles. e) R_{mic} as a function of the ML concentration in formulations containing 18% w/v P407 and 4% w/v ciprofloxacin, where R_{mic} was determined via SAXS (Figure S9.1a,b , Supporting Information). Dashed line indicates a 1:1 molar ratio of CIP:ML. Data was replicated using fresh samples on a lab-source Ganesha SAXS instrument and qualitatively matches that presented here (Figure S9.1b,c, Supporting Information) f) Rheology data showing similar gelation temperatures and gel moduli for formulations containing ciprofloxacin and ML.

Subsequently, a rigorous application of DFT was employed to identify the most thermodynamically stable conformation of the complex (Table S6.3, Supporting Information). Hydrogen bonding emerged as the paramount force driving the formation of this pseudo-surfactant, as substantiated by the N–H•••O bond distance of 1.658 Å (Figure 3b). Corroborative evidence from the Noncovalent Interaction (NCI) analysis (Figure 3c) elucidates robust attractive interactions, as shown by the blue interfacial region between ML's carbonyl group and ciprofloxacin's secondary amine group. Furthermore, the NCI analysis also revealed π-alkyl interactions between the alkyl chain of ML and the quinolone ring of ciprofloxacin, underscoring their contribution to conformational stabilization.

The computational predictions, which pointed to the formation of a pseudo-surfactant between ML and ciprofloxacin in a P407 micelle, were corroborated by experimental results on the structure of the P407 formulations obtained using SAXS (Figure 3d). Adding 4% w/v (40 mg mL^{-1}) ciprofloxacin to 18% w/v P407, i.e., [P407 + cip], did not dramatically alter the micelle size or gel structure at 35 °C. The micelles were packed onto an FCC lattice with an approximate radius of 110 Å – nearly identical to the 109 Å for [P407] (Figure 3d). This result was unsurprising, given that ciprofloxacin has a relatively high aqueous solubility (≈36 mg mL^{-1}).[24] Interestingly, while ML or ciprofloxacin alone was not incorporated into the P407 micelles, their combination, i.e., [P407 + cip + 2% ML], significantly increased the

micelle radius by over 30 Å (Figure 3d). Adding this combination also changed the relative peak intensities, including notable amplification of higher-order peaks and reduction of the (111) peak (see Section S8 for further discussion, Supporting Information). These results suggested that the two molecules interacted with each other, such that micelle incorporation was favored when combined. SAXS measurements also quantified the stoichiometry of ML and ciprofloxacin during the pseudo-surfactant formation on formulations with 18% w/v P407 and 4% w/v ciprofloxacin and with amounts of ML increasing from 0.1 to 4.7% w/v (Figure 3e; Figure S9.1, Supporting Information). The average radius of the micelles continued increasing as ML was added, until the molar ratio of ciprofloxacin: ML reached 1:1, and subsequently plateaued at higher ML concentrations, indicating a 1:1 stoichiometry for the ML-ciprofloxacin pseudo-surfactant. Promisingly, the [P407 + cip + 2% ML] formulation underwent a solution-to-gel transition between room temperature and body temperature, and formed a gel with similar moduli to that of [P407] and [P407 + cip] (Figure 3f; Figure S10.1, Supporting Information).

The DFT calculation, pointing to the importance of hydrogen bonding as a driving force for the pseudo-surfactant formation, was corroborated experimentally by SAXS performed on a formulation containing 18% w/v P407, 2% w/v ML, and a 1:1 molar ratio of ML:ammonium chloride (NH_4Cl) (Figure S9.2, Supporting Information). Ammonium chloride has a high aqueous solubility (>30% wt.)[25] and possesses a protonated amine, as does ciprofloxacin, and therefore was not expected to incorporate into the micelle if added in isolation but should exhibit similar interactions with ML if H-bonding contributes to the pseudo-surfactant formation. Consistent with this hypothesis, combining ML with NH_4Cl increased the micelle size by over 30 Å (Figure S9.2, Supporting Information), similar to the [P407 + cip + 2% ML] formulation.

2.3. The Copresence of ML and Ciprofloxacin Enhanced Transtympanic Drug Permeation but ML does not Act as a CPE Alone

The transtympanic drug flux was measured ex vivo across intact chinchilla TMs – a previously developed model for TM permeation.[7,14b,26] Here, three formulations, each containing 18% w/v P407 and 4% w/v ciprofloxacin: [P407 + cip], [P407 + cip + 2% ML], and [P407 + cip + 3CPE(SDS)] were tested. The 3CPE(SDS) is the best-in-class CPE combination for transtympanic drug delivery.[7,14b,26] The amount of ciprofloxacin that permeated across intact TMs to the middle ear side was sampled for 48 h and quantified using high-performance liquid chromatography (HPLC).

Drug permeation within the first 12 h was minimal for all groups (<0.2%). After 12 h, the drug permeation for both [P407 + cip + 3CPE(SDS)] and [P407 + cip + 2% ML] increased slightly relative to the baseline formulation [P407 + cip] (**Figure 4a**). This trend became more significant after 48 h, where 2.4 ± 0.6% of ciprofloxacin in [P407 + cip] permeated through the TM, while the addition of 3CPE(SDS) and 2% w/v ML more than doubled that amount, achieving 6.3 ± 1.0% ($p < 0.01$ vs [P407 + cip]) and 6.6 ± 1.2% ($p < 0.01$ vs [P407 + cip]), respectively. Note that the permeation enhancement achieved by [P407 + cip + 2% ML] was 3.6-fold to that previously reported for 2% w/v SDS (dotted line, Figure 4a).[14b] However, below, we prove that ML does not act as a CPE alone in this case.

To assess the permeation enhancement from only ML, in the absence of ciprofloxacin (hence no formation of pseudo-surfactant), a method that does not rely on quantifying the concentration of ciprofloxacin was required. Hence, we introduced the electrochemical impedance measurement of SLB[27] to assess lipid membrane integrity as a surrogate for drug permeation, since lipid bilayers constitute the most likely path of drug diffusion through the stratum corneum[3] and impedance measurements have been used extensively in studies on transdermal delivery.[14a,28] Furthermore, we show that the enhanced permeation does not occur in the absence of P407, highlighting the importance of the designed environment to enable the pseudo-surfactant formation.

The SLB was formed by 1-palmitoyl-2-oleoyl-glycero-3-phosphocholine (POPC), a widely used phosphatidylcholine model lipid, to recapitulate the phospholipids present in cell membranes.[29] The SLB was formed on top of a gold electrode that was coated with a biocompatible conducting polymer layer, poly(3,4-ethylenedioxythiophene)-poly(styrene sulfonate) (PEDOT:PSS) (Figure 4b; Figure S11.1, Supporting Information).[27,30] In the absence of SLB, the electrochemical impedance spectroscopy (EIS) signal exhibited a "hockey stick" shape over the frequency range of 1 to 10^6 Hz (dotted black line in Figure 4b), representing a capacitance-like behavior (representative of the PEDOT:PSS layer) at low frequencies and a resistor-like behavior (representative of the electrolyte solution) at high frequencies.[31] When the SLB was formed, the EIS signal shifted to a "chair" shape (represented as a solid yellow line in Figure 4b) which is a signature of the RC circuit (resistor–capacitor in parallel) shape of SLB.[31] By fitting this data to an equivalent circuit (Figure 4b), the SLB's resistance change after exposure to the formulations can be determined. A decrease in the impedance value indicates enhanced permeation across the SLB, and vice versa.

To minimize the mechanical perturbation to the SLB, which renders the EIS readings unreliable, diluted solutions of the aforementioned hydrogel formulations (100-fold in 0.9% NaCl) were used to treat the SLB (therefore the percentage of CPEs were temporarily omitted in figure panels). The treatment of diluted [P407] or [P407 + cip] (Figure 4c,d) maintained the SLB impedance profiles. Interestingly, diluted [P407 + ML] increased the SLB impedance by 38 ± 12% (Figure 4c,d), hinting at a lower SLB permeability, likely due to the physisorption of ML onto the SLB. In contrast, diluted formulations containing SDS (including [P407 + SDS], [P407 + cip + SDS], [P407 + 3CPE(SDS)], and [P407 + cip + 3CPE(SDS)]) all led to the destruction of the SLB, as indicated by the impedance profiles that matched an SLB-free device (Figure 4c; Figure S11.2, Supporting Information).

While [P407 + cip] or [P407 + ML] did not reduce the SLB impedance, the diluted [P407 + cip + ML]) caused a notable decrease by 90 ± 3% in the SLB impedance (Figure 4c). Unlike the SDS-containing formulations, [P407 + cip + ML] maintained the chair-like EIS profile (Figure 4d), indicating enhanced permeation, not destruction, of the SLB. These results thus hinted at the improved biocompatibility of the ML-containing formulations

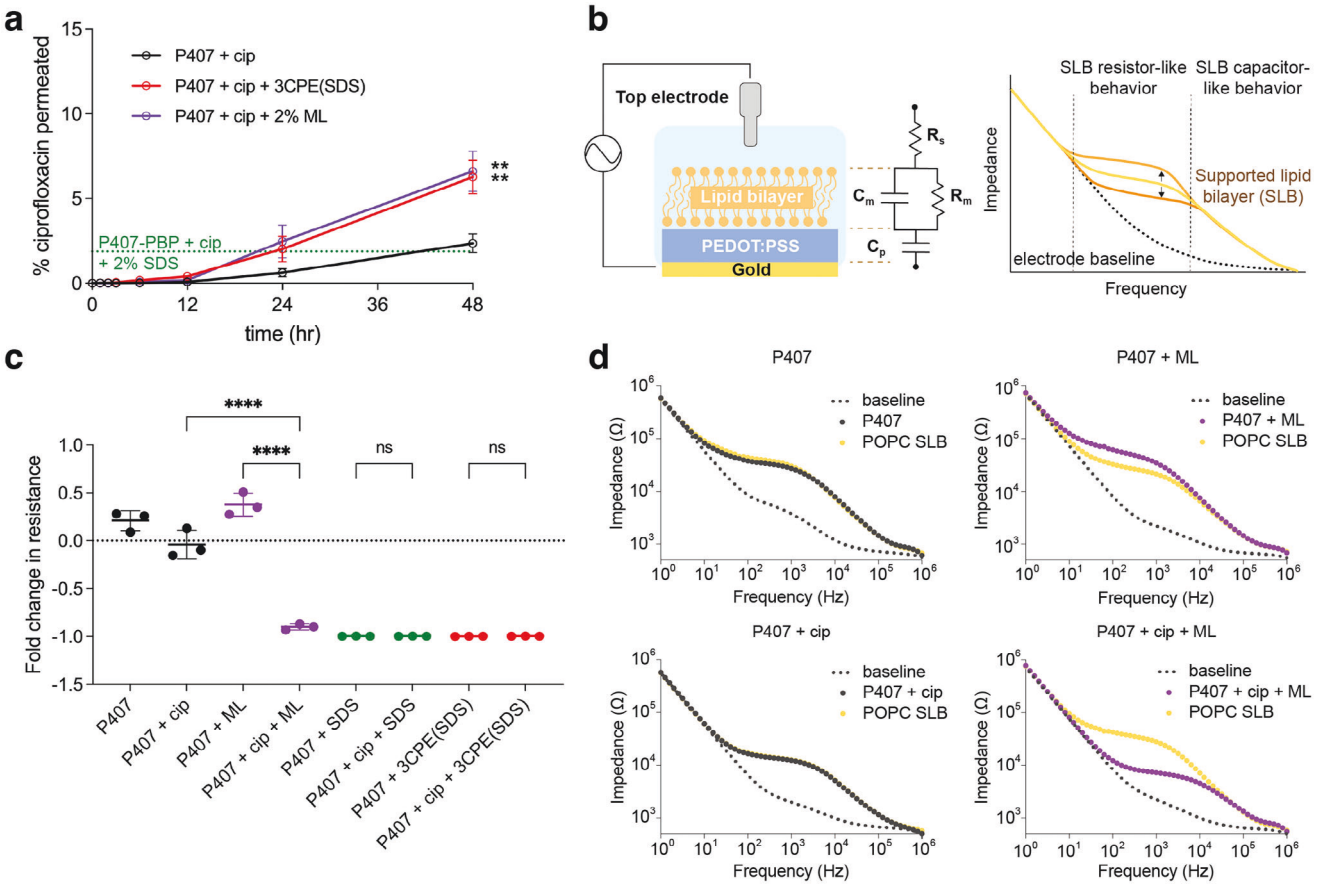

Figure 4. The permeation enhancement effects of ML. a) The ex vivo cumulative permeation of ciprofloxacin across healthy chinchilla TMs for hydrogels containing 18% w/v P407, 4% w/v ciprofloxacin, and various CPEs ($n = 4$). Data are mean ± SD; statistical analysis was performed using two-way analysis of variance (ANOVA) with Dunnett's test versus [P407 + cip], $^{**}p < 0.01$. b) Left: an illustration of the supported lipid bilayer (SLB) formed on a PEDOT:PSS-coated electrode and its equivalent electrical circuit. Right: representative impedance measurements taken for the SLB-free electrode (baseline) and the as-formed 1-palmitoyl-2-oleoyl-glycero-3-phosphocholine (POPC) SLB. c) The fold changes in the SLB impedance before and after the treatment with the hydrogel formulations calculated by fitting the electrochemical impedance spectroscopy (EIS) data using the sample circuit shown in [b]. Data are mean ± SD, $n = 3$; statistical analysis was performed using one-way ANOVA with Tukey's test, ns = non-significant, $^{****}p < 0.0001$. d) Representative microelectrode EIS measurements before SLB formation (baseline), after SLB formation (POPC SLB), and after the SLB was incubated with diluted [P407], [P407 + cip], [P407 + ML], or [P407 + cip + ML] formulation.

compared to those containing SDS, to be confirmed later. Additionally, the contrast between the impedance of the SLBs treated with [P407 + cip + ML] and that of [P407 + cip] or [P407 + ML] pointed to the effect of the ML-ciprofloxacin pseudo-surfactant on disrupting the structural integrity of the lipid bilayers.

2.4. A Hydrogel Formulation Containing the ML-Ciprofloxacin Pseudo-Surfactant Cured AOM in Chinchillas

The formulation's efficacy was tested for local antibiotic delivery in vivo in chinchilla models infected with non-typeable *Haemophilus influenzae* (*NTHi*) (**Figure 5a**). After establishing the AOM infection, a one-time administration of the formulations was performed (Figure 5b). The formulations were placed as close to the TM as possible in a noninvasive fashion. The best-in-class CPE combination, 3CPE(SDS), was used as a benchmark. While administration of the [P407 + cip + 2% ML] was facile, the [P407 + cip + 3CPE(SDS)] formulation was difficult to administer,[26] because it could transition from a liquid to a hydrogel as it was being extruded, before reaching the TM (Figure S12, Supporting Information).

After a single-dose injection, the [P407 + cip + 2% ML] formulation eradicated AOM in 83% of the treated animals ($n = 6$) within the first 24 h (Figure 5c), and the treatment effect was maintained through day 7 ($p < 0.01$ vs untreated). The colony-forming unit (CFU) count of *NTHi* culture recovered from the middle ear fluid (MEF) showed a sharp decrease on day 1 after the treatment, from a median of 1.75×10^7 to 0 (Figure 5d), and the low CFU count was maintained throughout the 7-d treatment. NTHi was not eradicated in one of the six animals treated with [P407 + cip + 2% ML], but the MEF CFU count for this animal did show a 3-log reduction from day 0 to day 7, corresponding to a 99.9% reduction of the bacterial count in the middle ear, which has been considered an indication of cure elsewhere.[26,32] By contrast, treatment with [P407 + cip + 3CPE(SDS)] ($n = 4$) led

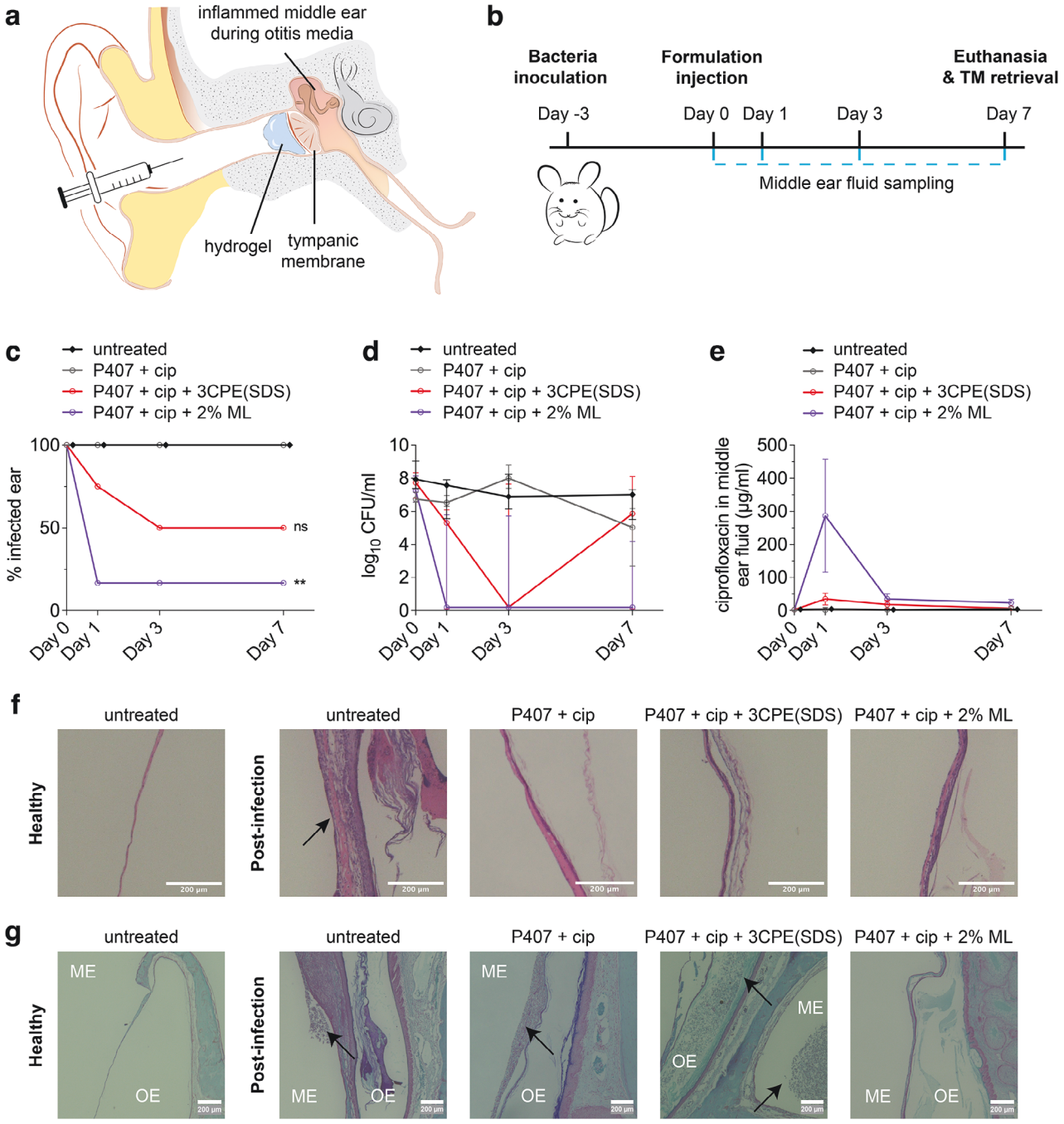

Figure 5. The in vivo application, treatment efficacy, pharmacokinetics, and biocompatibility of the hydrogel formulations. a) A scheme showing the injection of the hydrogel formulation through the outer ear canal, for noninvasive and local delivery of antibiotics across intact tympanic membrane (TM) for treatment of acute otitis media (AOM). b) The study timeline for the in vivo chinchilla AOM model. c) The percentage of chinchilla ears with nonzero colony-forming unit (CFU) counts of *non-typeable Haemophilus Influenzae* (*NTHi*) in the middle ear fluid (MEF) before (i.e., Day 0) and after receiving the treatment of [P407 + cip] ($n = 4$), [P407 + cip + 3CPE(SDS)] ($n = 4$), and [P407 + cip + 2% ML] ($n = 6$), or no treatment ($n = 4$). Statistical analysis was performed using two-way ANOVA with Dunnett's test versus [untreated] for day 7, ns = nonsignificant, ** $p < 0.01$. d) The CFU count of *NTHi* in the MEF extracted from the same animals as in [c]. The Log_{10} CFU value of zero was represented as one instead of $-\infty$ for illustration purposes; data are median and interquartile range. e) The concentration of ciprofloxacin in the middle ear fluid extracted from the same animals as in [c]; data are mean ± Standard Error of Mean (SEM). f) Representative images showing sectioned TM from *NTHi*-infected and healthy chinchillas after 7 d of treatment, with hematoxylin & eosin (H&E) staining, black arrow indicates regions of infiltrating leukocytes. The average thickness for a healthy untreated TM was measured to be 12 ± 3 µm ($n = 1$). The average thickness for infected TM was measured to be 49 ± 46, 42 ± 21, 101 ± 70, and 36 ± 10 µm, after receiving no treatment or treatment with [P407 + cip], [P407 + cip + 3CPE(SDS)], and [P407 + cip + 2% ML], respectively ($n = 3$ for [P407 + cip], $n = 4$ for all other groups), scale bar = 200 µm. g) Representative images showing section TM from *NTHi*-infected and healthy chinchillas after 7 d of treatment, with Gram staining, black arrow indicates clusters of bacteria, ME: middle ear, OE: outer ear, scale bar = 200 µm.

to a 50% cure rate, with a median CFU count of 7.25×10^5 on day 7. The animals that were untreated ($n = 4$) or treated with only [P407 + cip] ($n = 4$) remained 100% infected through day 7, with a median CFU count of 1.02×10^7 and 1.06×10^5 on day 7, respectively.

Additionally, a formulation containing [P407 + cip + 3CPE(ML)], a new CPE combination consisting of 1% w/v ML, 2% w/v limonene, and 0.5% w/v bupivacaine (directly substituting SDS in 3CPE(SDS)), exhibited similar hydrogel properties and comparable in vivo efficacy to [P407 + cip + 2% ML] which was far superior to that of [P407 + cip + 3CPE(SDS)] (Figures S5.2,S10.1,S10.2 and S13, Supporting Information).

In addition to high cure rates, the concentration of ciprofloxacin in the MEF over the course of treatment indicated a clear enhancement of drug permeation across the TM with the addition of 2% w/v ML (Figure 5e). The drug concentration in animals treated with [P407 + cip + 2% ML] peaked on day 1, at 286 ± 170 μg mL^{-1} ($p = 0.35$ vs untreated). Meanwhile, the drug concentration in animals treated with [P407 + cip + 3CPE(SDS)] and [P407 + cip] peaked at 35 ± 18 μg mL^{-1} ($p = 0.99$ vs untreated), and 4 ± 3 μg mL^{-1} ($p = 0.99$ vs untreated) on day 1, respectively. By day 7, much of the ciprofloxacin in the middle ear had been cleared, and the MEF drug concentration from animals treated with [P407 + cip + 2% ML], [P407 + cip + 3CPE(SDS)], and [P407 + cip] was 30 ± 14, 7 ± 3, and 7 ± 2 μg mL^{-1}, respectively.

Infected chinchilla bullae were retrieved after the 7-d course of treatment for histochemical staining and imaging under a cross-sectional view (Figure 5f,g). Compared to a healthy TM, an infected TM exhibited inflammatory signs and a greater thickness (Figure 5f). The treatment with [P407 + cip], [P407 + cip + 3CPE(SDS)], or [P407 + cip + 2% ML] reduced the inflammatory signs but failed to bring the TMs to pristine conditions (Figure 5f). Gram staining suggested the presence of clusters of bacteria in the middle ear or near the TM in the groups that were untreated, treated with [P407 + cip], or treated but uncured with [P407 + cip + 3CPE(SDS)]. Such bacteria clusters were absent from the animals treated with [P407 + cip + 2% ML] (Figure 5g).

Promisingly, ML demonstrated much-improved biocompatibility compared to SDS or 3CPE(ML). Cytotoxicity was first assessed in vitro using primary human adult fibroblast cells and PC12 (a pheochromocytoma cell line used in neurotoxicity testing) (Figures S14.1,S14.2, and S14.3, Supporting Information). Meanwhile, the P407 hydrogel had minimal cytotoxicity, but ciprofloxacin showed evident cytotoxicity at 4% w/v. Since the intended application for this hydrogel formulation is to treat AOM via a one-time administration for a short course of duration, an in vivo biocompatibility test was carried out for 7 d to match this anticipated short treatment. When assessed for tissue toxicity, healthy chinchilla TMs treated with [P407 + cip], [P407 + cip + 3CPE(SDS)], and [P407 + cip + 2% ML] for 7 d exhibited only slight inflammations, showing a thickness of 11 ± 5, 38 ± 9, and 38 ± 5 μm, respectively ($n = 1$) (Figure S15, Supporting Information). The slight inflammations were likely as a result of the exfoliating effect of the surfactant and pseudo-surfactant,[33] and no other histological abnormalities were witnessed.

3. Discussion

A novel strategy leveraging an excipient-drug combination as a pseudo-surfactant to enhance drug permeation across biological barriers was developed. This led to the local and noninvasive treatment of AOM in a chinchilla model. A distinct advantage of this strategy was that the treatment formulation contained only FDA-approved ingredients, including a thermoresponsive polymer P407, the antibiotic ciprofloxacin, and a permeation enhancer ML. P407 and ciprofloxacin have both been used in FDA-approved otic and intratympanic products,[12b,13,34] and ML has been used in FDA-approved topical pharmaceuticals, e.g., fentanyl patch, testosterone patch.[35] The formulation thus points to an accelerated path to clinical adoption. A single dose of the formulation delivered the entire course of the regimen, thus addressing a main challenge faced by the current standard of care using oral antibiotics – poor patient compliance with the multi-day and multi-dose administration.[10] The local, transtympanic delivery method also avoids systemic exposure to antibiotics for this extremely prevalent pediatric condition, alleviating side effects and mitigating the potential for antibiotic resistance.

To achieve trans-tympanic permeation, gelation, and sustained drug release simultaneously, this work harnessed a fresh concept of drug-excipient pseudo-surfactant, which was enabled by a designed environment of P407 micelles. While other CPE-containing hydrogel formulations have achieved similar transtympanic delivery efficiency,[7,14,26] these systems often require custom-synthesized and, thus, non-FDA-approved polymers to formulate the hydrogel. The previously reported chemical modifications were required due to the disruption of common CPEs, like SDS, on the gelation properties of P407, by preventing the polymer micellization.[4c,22e] In contrast, we demonstrated that the ML-ciprofloxacin pseudo-surfactant maintained the gelation temperature and gel modulus of the P407 hydrogel while enabling trans-tympanic flux that was sufficient to cure AOM in chinchillas. The use of unmodified P407 in this formulation could thus help accelerate its clinical translational pathway by removing the need for gaining regulatory approval for the use of a polymer that has not been subject to clinical trials previously. Nevertheless, systematic clinical studies are likely warranted prior to the adoption of the reported formulation in pediatric clinics. Such clinical studies typically start with a safety assessment and proceed to efficacy verification. Despite the pediatric indication that the reported formulation targets, safety assessment studies will likely initially focus on adult subjects, which may pose a distinct challenge for the clinical translation of the formulation as adult patients of otitis media are uncommon. While this challenge is faced by all formulations aiming to treat otitis media with locally delivered antibiotics, an advantage of the reported formulation is that, compared to the best-in-class formulation, which requires a multi-component 3CPE(SDS), the reported use of ML alone likely reduces the number of permutations that require testing in future clinical studies, thereby accelerating the development to adoption pathway.

Detailed computational simulation and structural analysis proved the formation of the pseudo-surfactant between ML and ciprofloxacin. The ML-ciprofloxacin association in a P407 micelle was predicted by MD simulations and corroborated by SAXS

experiments. Detailed SAXS analyses revealed an enlargement of the P407 micelle upon adding ciprofloxacin and ML simultaneously (with a micelle radius of 143 Å) while [P407], [P407 + cip], and [P407 + 2% ML] all led to a similar micelle radius (≈109 Å), indicating that the interaction between ciprofloxacin and ML led to their inclusion in the P407 micelles. DFT simulations suggested that hydrogen bonding and π-alkyl interactions contributed significantly to the complexation of ciprofloxacin and ML within micellar environments, which SAXS also corroborated. This pseudo-surfactant, in turn, significantly improved drug permeation across intact TMs, as we demonstrated in ex vivo permeation studies using intact healthy chinchilla TMs. The permeation enhancement could not be achieved by ML or ciprofloxacin alone, as shown using impedance measurements on supported lipid membranes.

Importantly, the permeation enhancement led by the pseudo-surfactant contributed to its in vivo efficacy in treating otitis media. While the formulation containing a previously demonstrated effective combination of CPEs, [P407 + cip + 3CPE(SDS)], achieved a 50% cure rate, the new formulation [P407 + cip + 2% ML] eradicated NTHi in 5 out of 6 infected chinchillas and achieved more than 3-log reductions in the remaining 1 out of 6 animals, which was also considered an indication of cure elsewhere.[26,32] The formulation [P407 + cip + 2% ML] achieved a ciprofloxacin concentration of 286 ± 170 μg mL^{-1} in the middle ear fluid after day 1 of treatment, which was 2–3 orders of magnitude greater than the minimum inhibitory concentration for *NTHi*.[36] The drug concentration in the middle ear fluid remained high throughout the 7-d treatment, reaching 30 ± 14 μg mL^{-1} by day 7. Moreover, histology and cytotoxicity data both indicated favorable biocompatibility of ML compared to the previously used 3CPE(SDS). This was unsurprising as SDS has been reported to cause more skin irritation than most FAMEs,[1a] given its ability to extract lipids from the lipid lamellae[3a] while solubilizing the proteins in the stratum corneum.[37] In terms of ototoxicity, it has been shown that the previous leading 3CPE(SDS)-containing hydrogel caused minimal and temporal changes to the auditory response in chinchillas after application onto the tympanic membrane.[7] P407 has also been used in an FDA-approved otic suspension product, Otiprio, for treating otitis media (OM) patients undergoing tympanostomy tube placement (an artificial passage inserted onto the TM). Clinical trial results have indicated no formulation-related audiometric change to patients who were injected with this suspension product, which contained 6% ciprofloxacin and P407 hydrogel, into the middle ear.[38] Thus, this new hydrogel formulation was also expected to cause small changes to hearing, if any.

The single-CPE hydrogel formulation developed herein represented a step forward in transtympanic delivery technology for its simplicity, efficacy, and biocompatibility. Moreover, the reported hydrogel formulation has the potential to serve as a versatile platform for other types of therapeutic delivery commissions into the middle ear cavity. For example, patients experiencing chronic suppurative otitis media (CSOM) may suffer from chronic TM perforation,[39] and to encourage TM repair, hydrogels have been increasingly used as a medium for delivering growth factors and structural proteins, such as collagen and gelatin, that are required for epithelial tissue repair.[40]

In addition, the pseudo-surfactant reported in this work highlighted the importance of gauging the interactions among small-molecule drugs and excipients in developing multicomponent delivery vehicles. Given that ≈50% of all small-molecule drugs are formulated as ionizable salt,[41] the pseudo-surfactant approach could be broadly applicable to other FDA-approved compounds and help with new designs for delivering therapeutics across biological barriers, ranging from transdermal and transbuccal to intestinal delivery.

4. Conclusion

An ototopical formulation for the local delivery of ciprofloxacin across intact TMs was developed in this work. Successful single-dose treatments of *NTHi*-induced AOM were achieved in chinchilla models, through a non-invasive injection of the formulation to the outer ear canal. This formulation contained the thermoresponsive P407 hydrogel, the antibiotic ciprofloxacin hydrochloride, and ML – a newly selected transtympanic CPE. Unlike a previously used anionic surfactant, SDS, ML exhibited minimal interference with the micellization and gelation of P407. Therefore, ML was able to preserve the gelation properties and the drug release profile of the hydrogel. Further, structural characterization of the formulations using SAXS and DLS suggested that ML interacted with ciprofloxacin to form a pseudo-surfactant that incorporated into P407 micelles, which was corroborated by MD simulations and DFT calculations. Moreover, the formation of pseudo-surfactant likely contributed to the heightened disruption to lipid bilayers exhibited by the ML-ciprofloxacin combination, relative to that produced by either ML or ciprofloxacin alone in P407 hydrogel, as measured in EIS studies. These results highlight that for a multicomponent hydrogel formulation as such, harnessing the drug-excipient interactions could be useful for tuning the physical properties and improving the therapeutic efficacy of the formulation.

5. Experimental Section

Materials: All hydrogels were prepared using Kolliphor Poloxamer 407 which was obtained from Sigma-Aldrich and used without further purification. Methyl laurate (≥98%) and (R)-(+)-limonene (≥97%) were also obtained from Sigma-Aldrich, and ciprofloxacin hydrochloride (≥98%, referred to as ciprofloxacin in the sections above) and bupivacaine hydrochloride were obtained from Millipore Sigma. Sodium dodecyl sulfate was obtained from VWR for release studies (≥99%) and from Sigma-Aldrich for structural studies (≥99%); however, no differences were observed between these two suppliers. For the structural analysis, ammonium chloride was obtained from Fisher Scientific and used without further purification.

Hydrogel Formulations: Hydrogels were fresh prepared for each experiment. P407 powder was dissolved in MilliQ water to a final concentration of 18% w/v at 4 °C. To this hydrogel, drugs and various CPEs were added. For [P407 + cip], ciprofloxacin hydrochloride powder was added to a final concentration of 4% w/v (40 mg mL^{-1}). In addition, formulations containing both ciprofloxacin hydrochloride and CPEs were created, with these final concentrations: [P407 + cip + ML] contained 2% w/v methyl laurate; [P407 + cip + 3CPE(SDS)] contained 0.5% w/v bupivacaine hydrochloride, 1% w/v SDS, and 2% w/v limonene; [P407 + cip + 3CPE(ML)] contained 0.5% w/v bupivacaine hydrochloride, 1% w/v methyl laurate, and 2% w/v limonene. For the in vitro release study, individual components of 3CPE(SDS) were also singly added to [P407 + cip].

Rheology: Small-amplitude oscillatory rheology was used to probe the dynamic moduli of the 18% w/v formulations as a function of temperature. Measurements were performed on an Anton Paar 302-e rheometer using a double-gap geometry with a constant frequency of 1 rad s^{-1}, strain amplitude of 1% and heating rate of 1 °C min^{-1}. Samples were loaded at 5 °C and allowed to equilibrate for 10 min prior to the temperature ramp from 5 to 50 °C. This procedure has been used previously to determine rheological transition temperatures in P407-based formulations and transition temperatures were quite reproducible, with a standard deviation of 1 °C or less across three replicates.[16a]

Differential Scanning Calorimetry (DSC): The thermodynamics of the micellization process were probed using a TA instruments Q1000 DSC. Approximately 20 µL of the 18% w/v formulations were loaded into Tzero hermetically sealed pans. The samples were equilibrated at 7 °C for 10 min prior to heating at 1 °C min^{-1} up to 50 °C. The raw differential heat flow data were baseline subtracted using a linear baseline. This ramp rate and thermal protocol has been used prior to determine the micellization temperature and enthalpy of micellization. In previous work, the micellization temperature varied by less than 1 °C across three replicates and the enthalpy of micellization, determined by integrating the heat flow curve, varied by less than 2 J $g_{polymer}{}^{-1}$.[16a]

Small-Angle X-Ray Scattering (SAXS): Synchrotron SAXS measurements were conducted at Sector 5-ID-D of the Advanced Photon Source (APS) at Argonne National Lab. Measurements were conducted using a wavelength of 0.793 Å, allowing for an accessible q-range from 0.002 to 4.4 $Å^{-1}$ across three detectors. For this work, data were truncated to highlight features of interest between 0.02 and 0.1 $Å^{-1}$. Samples were loaded into 1.5-mm quartz capillaries within a custom multi-capillary temperature stage and scanned every 5 °C from 5 to 50 °C following a 10-min equilibration period at each temperature. Select samples containing ML and ciprofloxacin hydrochloride were scanned at 37 °C. Each scan used a 1 s exposure time and every sample was scanned in three positions vertically along the capillary. The 2D patterns were visualized using DataSqueeze[42] and azimuthally integrated to yield 1D traces. Ordered phases were identified based on the position of Bragg peaks within the 1D traces.

Dynamic Light Scattering (DLS): Samples were prepared with a P407 concentration of 1% w/v. The ratio of P407 to small molecules was kept constant between the concentrated (18% P407) and dilute samples. All components were dissolved in HPLC-grade water at 4 °C. Samples were then heated to 37 °C to allow for micelle formation prior to being passed through a 0.22-µm hydrophilic polypropylene filter. The filtered solutions were loaded into glass tubes for measurements.

Multi-angle DLS was performed on a Brookhaven BI-200SM instrument with a 637-nm laser. Throughout the measurements, samples were submerged in a circulating decalin bath maintained at 37 °C. Autocorrelation functions were collected for 5 min over a range of 0.5 µs – 10 ms at 60°, 75°, 90°, 105°, and 120°. Regularized positive exponential sum (REPES) analysis was used to determine that all data could be described by a single relaxation mode. Hydrodynamic radii were determined by fitting the data at each angle to a second cumulant expansion. For each sample, there was a strong linear relationship between the first cumulant versus scattering angle squared, indicating a diffusive process. The slope of this line corresponds to the mutual diffusion coefficient (D_m), which in these dilute solutions is equivalent to the tracer diffusion coefficient (D_t). The tracer diffusion coefficient can be related to the hydrodynamic radius using the Stokes–Einstein relation.

Optical Microscopy: Optical microscopy was used to visualize the size of ML droplets within hydrogels containing 18% P407 with 2% ML. Measurements were conducted on an Olympus BX53 microscope. Samples were preheated to 37 °C before being transferred to a glass microscope slide. Samples were then placed into a Linkam T95 temperature controller and imaged at 37 °C.

Fully Atomistic Molecular Simulation (MD): Fully atomistic MD simulations were performed with the NAMD 2.14 molecular dynamics software.[43] The mTIP3P[44] and CHARMM36[45] force fields were used to model water and polymer interatomic interactions, respectively. The full molecular model for the aqueous solution of P407, constructed by CHARMM-GUI (http://www.charmm-gui.org) v3.7,[46] comprises four full-length P407 polymer chains, each with a central 56-unit polypropylene glycol block flanked by two 101-unit polyethylene glycol blocks. For the aqueous solution of P407, the initial configuration was energetically minimized for 20 ps then followed by a 250 ps NVT MD equilibration at 310 K. During the equilibration, the atoms on the polymer backbone were restrained using a harmonic potential with a 1 kcal mol^{-1} $Å^{-2}$ force constant. Production simulations were run in NPT ensemble for 10 ns at 310 K and 1.0 1325 bar. After the [cip + ML] complex was incorporated into the micelle formed by P407, the simulation was run in NPT ensemble for 10 ns at 310 K and 1.0 1325 bar. The aqueous solution of [cip+ML] was solvated in water with 10 Å of padding around the complex in each dimension using the Solvate plugin in Visual Molecular Dynamics (VMD).[47] The simulation was run in NPT ensemble for 10 ns at 310 K and 1.0 1325 bar. All the MD simulations were visualized using VMD.

Conformation Generation: Snapshots of the [cip + ML] complex were extracted from the MD simulation at intervals of 2 ps, resulting in a total of 5000 conformations. Additional 5000 conformations of [cip + ML] were generated using a genetic algorithm implemented in Open Babel.[48] Each conformation was then optimized at the GFN2-xTB[49] level of theory with the xtb[50] and CREST[51] programs. The 10 conformations exhibiting the lowest energy were subsequently identified for in-depth electronic structure analysis.

Density Functional Theory (DFT) Study: All DFT calculations were performed with the ORCA 5.0.3 quantum chemistry package.[52] Geometry optimizations were performed at the ωB97X-D3[53] level of theory. All atoms were described with a def2-TZVP basis set.[54] Analytical frequency calculations were performed at the same level of theory to characterize all stationary points (no imaginary frequencies). Noncovalent interaction (NCI) analysis was performed based on the wavefunction information from DFT calculations with the NCIPLOT 4.0 program.[55]

In Vitro Drug Release: The release of ciprofloxacin hydrochloride from each hydrogel formulation was measured using a Transwell diffusion system. Semipermeable membrane inserts (12-mm Transwell insert with a polyester membrane with 0.4-µm pore size, Corning 3460) were placed in 12-well culture plates, which acted as receiving chambers. Each hydrogel formulation was added to the insert at a volume of 200 µL/insert and allowed to gel for 20 min in an incubator kept at 37 °C. The control group, 4% ciprofloxacin in water, was added at the same volume to probe the inherent diffusivity of the Transwell insert. Next, 1.5 mL of prewarmed 0.9% NaCl saline was added to the receiving chamber. At each time point (1, 2, 3, 6, 12, 24, 48, 72, 120 h), the saline in the receiving chamber was retrieved for analysis and each insert was placed into a new well with the same amount of fresh saline (i.e., 1.5 mL). Samples were diluted in MilliQ water as needed, filtered with a 0.45-µm (pore size) PTFE membrane, then analyzed by HPLC to determine the concentration of ciprofloxacin hydrochloride. For these measurements, HPLC-grade acetonitrile, methanol, and water were obtained from Fisher Chemical and HPLC-grade trifluoroacetic acid (TFA) was obtained from Sigma-Aldrich. The HPLC was performed on a Shimadzu LC-2030C 3D with a C18 column, 4.6×100 mm, 2.7 µm (Agilent). The mobile phase contained acetonitrile with 0.1% TFA (solvent A) and water with 0.1% TFA (solvent B). Samples (10 µl) were eluted with a gradient from A:B = 90:10 v/v to 10:90, then back to 90:10, under a flow rate of 1 mL min^{-1}. Eluents were measured for UV–vis absorbance at 270 nm.

Ex Vivo Drug Permeation Study: TMs from healthy chinchillas were harvested for ex vivo drug permeation study. Chinchillas were euthanized under CO_2 inhalation in accordance with IACUC guidelines, thereafter the auditory bullae were removed from the skull. Each bulla was excised to expose the middle ear chamber and the TM, which was carefully maintained intact in the tympanic ring. Immediately following dissection, the TMs were visually examined, and their electrical impedance was measured using a previously described protocol[14a] to test tissue integrity. Excised bullae were placed vertically in sterile 12-well plates, with the external ear canal facing upwards and the exposed middle ear chamber facing downwards and submerged in 3 mL of sterile 1x phosphate buffered saline. Formulations (200 µL) were injected with micropipettes into the external ear canal. Bullae were kept in a humid chamber and placed in a 37 °C incubator. At predetermined time points (1, 2, 3, 6, 12, 24, 48 h), the saline

solutions from the well plate were sampled and fresh sterile saline was added to ensure the infinite sink conditions. The samples were collected until 48 h to avoid complications from tissue degradation thereafter. The drug concentration was determined using HPLC. Sample aliquots were diluted with HPLC grade methanol and sonicated for 10 min for protein precipitation, and then filtered with a 0.45-µm pore size membrane before HPLC.

Microelectrode Fabrication: To fabricate the microelectrodes, gold contact pads were first patterned on silicon wafer using photolithography. Then, a layer of silicon oxide was deposited on the wafer using plasma enhanced chemical vapor deposition. A second series of photolithography was conducted to outline the position of the electrodes followed by reaction ion etching to specifically remove the silicon oxide above the gold contact pads. The mixture of PEDOT:PSS (Heraeus) with 1% v/v (3-glycidyloxypropyl)trimethoxysilane was spin-coated on the wafer at 4000 rpm followed by 30 min of annealing on a hot plate maintained at 140 °C. A third series of photolithography was conducted to specifically remove the PEDOT:PSS above the deposited silicon oxide using a sacrificial Germanium layer, as detailed in a protocol reported previously,[56] resulting in microelectrodes consisted of a layer of gold contact pads and PEDOT:PSS (Figure S2.1, Supporting Information). A small well to contain the buffer solutions was made from polydimethylsiloxane and affixed over the device prior to any electrical measurements.

Lipid Bilayer Formation: Small unilamellar liposomes of 1-Palmitoyl-2-oleoyl-glycero-3-phosphocholine (POPC, purchased from Avanti Polar Lipids) were prepared via extrusion. POPC dissolved in chloroform (purchased from Avanti Polar Lipids) had the solvent removed first using nitrogen gas, then kept under vacuum for 4 h to fully evaporate all the solvent. The POPC thin film remaining on the glass vial was then rehydrated in Tris buffer (10×10^{-3} M Tris and 150×10^{-3} M KCl at pH 7.4), vortexed, and extruded 15 times through a 100-nm Nucleopore polycarbonate membrane (Whatman Nucleopore) using a mini extruder (Avanti Polar Lipids). Prior to forming the SLB via vesicle fusion, the PEDOT:PSS electrode device was soaked in DI water overnight, then treated with light oxygen plasma (Harrick Plasma PDC-32G, 7.2 W, 350 Micron, 1 min) to provide sufficient hydrophilicity to allow the self-assembling of POPC liposomes into SLBs.[27] The PEDOT:PSS electrodes were first measured for baseline EIS signal. Then, POPC vesicles were added onto the electrode surface and incubated for 60 min in Tris buffer for the formation of SLB. The buffer was then exchanged to 0.9% NaCl and the SLB was allowed to equilibrate for 20 min prior to EIS measurement for SLB signal. Then, hydrogel formulations were dissolved 1:100 in 0.9% NaCl and added to the SLBs. After 30-min treatment, the SLBs were rinsed with 0.9% NaCl and equilibrated for another 30 min prior to the last EIS measurement.

Electrochemical Impedance Spectroscopy (EIS) Measurement and Data Analysis: EIS measurements were performed using a potentiostat (Autolab PGSTAT128N). The EIS was monitored over the frequency range of 1 000 000–1 Hz for the applied AC voltage. The reference and counter electrode used were a commercially available Ag/AgCl electrode and a platinum mesh, respectively. PEDOT:PSS-coated Au electrodes were used as working electrodes. The measured impedance spectra were analyzed using the Metrohm Autolab NOVA software (v 2.1.6). EIS data were fitted to a RC circuit for the electrode baseline or a RC(RC) circuit for electrodes after SLB formation.

Animal Maintenance: Healthy adult chinchillas weighing 400–600 g were obtained from the Mutation Chinchilla Breeder Association (NY). All animal care and experiment activities were carried out in accordance with the protocol (#2018-0089) approved by the Institutional Animal Care and Use Committee (IACUC), in conjunction with the Center of Animal Resources and Education (CARE) Animal Use Guidelines at Cornell University.

Acute Otitis Media (AOM) Animal Model: NTHi was grown to the mid-log phase and diluted in sterile Hanks' balanced salt solution (HBSS). The solution (100 µL, 25–75 CFU) was inoculated directly into the middle ear of chinchillas through the bulla, using aseptic techniques. Once pathogen inoculation was completed, chinchillas were monitored, and their TMs examined via otoscopy. After middle ear infection was established (usually at 3 d post inoculation), 200 µL of the formulations were administered through the external ear canal using a soft-tipped 22-gauge angiocatheter (without needle, Monoject), and the animals underwent surgery for middle ear sample collection. The animals were anesthetized under isoflurane inhalation, placed in ventral recumbency, and had their tympanic bullae surgically prepped. A small surgical opening was created at the most palpable region of the tympanic bulla with a scalpel blade. Direct samples of the middle ear culture were obtained with sterile cotton swabs, and immediately streaked onto chocolate agar plates. The MEF was retrieved through the surgical opening with a 22-gauge angiocatheter (without needle) connected to a 1 mL tuberculin syringe, without hampering TM integrity. The MEF was sampled before the treatment on day 0, and after the administration of the formulations on day 1, day 3, and day 7. The MEF (10–20 µL) was diluted in HBSS with tenfold serial dilution and plated onto chocolate agar plates. The number of colonies was counted to calculate the CFU of NTHi, with the lower limit of detection being 100 CFU mL^{-1}.

Histology: Hydrogel formulations were administered to the external ear canal of healthy or infected chinchillas. Seven days after the administration, animals were euthanized under CO_2 inhalation in accordance with IACUC guidelines. The bullae were retrieved and excised to expose the TM, while the bone and tissue around the tympanic ring were carefully removed. The excised samples were immediately fixed in 10% neutral buffered formalin overnight. Decalcification, paraffin embedding, sectioning (5-µm-thick), and hematoxylin and eosin staining were performed by the Section of Anatomic Pathology at the Animal Health Diagnostic Center at Cornell University (Ithaca, New York, USA; fee for service), using standard techniques. Stained specimens were examined under light microscopy (VHX optical microscope, Keyence). The thickness of the TM was measured with Fiji.[57] Six measurements were taken for each specimen.

Cell Culture and Cytotoxicity: Adult primary dermal fibroblast cells (hFbs, ATCC PCS-201-012) were maintained in fibroblast basal medium (ATCC PCS-201-030) supplemented with low-serum growth kit (ATCC PCS-201-041) and 1% penicillin/streptomycin (Gibco 15-140-122). PC-12 cells (ATCC CRL-1721.1), isolated from pheochromocytoma, were maintained in F-12K medium (Gibco 21-127-022) supplemented with 2.5% fetal bovine serum (Gibco 16-000-044), 15% horse serum (Gibco 26-050-088), and 1% penicillin/streptomycin (Gibco 15-140-122). All cell cultures were maintained in an incubator kept at 37 °C and 5% CO_2.

For cytotoxicity testing, hFbs and PC-12 cells were seeded into 12-well plates at a cell density of 80 000 cells/well and incubated overnight prior to being treated with the various formulations. Small molecule compounds and CPEs (without P407) were directly dissolved in media, or dissolved in media with 1% v/v dimethyl sulfoxide (DMSO, Corning) in the case of ML to improve its solubility. After one day of culture, cell media were replaced with 1 mL fresh media containing the tested compounds. For formulations containing P407, 200 µL of the formulation was placed into a prewarmed sterile insert (12-mm Transwell insert with 0.4-µm pore polyester membrane, Corning 3460) and the insert was placed in a well with the cells and 1 mL fresh media. After 24 h of treatment, cell viability was measured with the WST-8 cell proliferation assay kit (Cayman Chemical 10 010 199) and the LIVE/DEAD viability/cytotoxicity kit (Invitrogen L3224). In brief, WST-8 mixture solution was freshly prepared and added to each well to a final concentration of 10% of the media volume. After 2–4 h of incubation at 37 °C, the media were collected from each well, centrifuged, and measured for absorbance at 450 nm in a plate reader. For live/dead staining, cells were incubated with calcein-AM (1×10^{-3} M) and ethidium homodimer (2×10^{-3} M) for 15–30 min at 37 °C and then imaged with a fluorescent microscope (Axiovert, Zeiss). Cell viability was calculated as (live cells)/(live cells + dead cells) * 100%.

Statistical Analysis: All drug permeation, drug release, and animal study data were presented as mean ± standard deviation (SD) unless otherwise mentioned in the respective figure legends. The CFU count of NTHi in the middle ear was presented as median ± interquartile range. Sample size is listed for each experiment in the respective figure legends. Statistical analyses were performed with the GraphPad Prism 9.4 software. Multiple group comparisons were performed using one-way analysis of variance (ANOVA) followed by Tukey's test. Multiple group comparison with two variables were performed using two-way ANOVA followed by Dunnett's test. Statistical significance was defined as $*p < 0.05$, $**p < 0.01$, $***p <$

0.001, ****$p < 0.0001$. For DLS, data taken at multiple angles for a single sample were fit to a linear regression and the reported errors are propagated from the 95% confidence interval of the slope value.

Supporting Information

Supporting Information is available from the Wiley Online Library or from the author.

Acknowledgements

S.S.L. and J.M.W. contributed equally to this work. This work was supported by grants from the National Institute on Deafness and Other Communication Disorders of the National Institutes of Health (grant R21DC019184), the Natural Sciences and Engineering Research Council of Canada (CGS-D) to S.S.L., the National Science Foundation Graduate Research Fellowship (grant 2237827) to J.M.W., the Smith Fellowship for Postdoctoral Innovation at Cornell University to Z.C. and S.D., the Eric and Wendy Schmidt AI in Science Postdoctoral Fellowship, a Schmidt Futures program, to Z.C. and the Partnership for Research and Education in Materials within the National Science Foundation (grant DMR-2122178) to A.G. The fabrication of microelectrodes was performed in part at the Cornell NanoScale Facility, a member of the National Nanotechnology Coordinated Infrastructure (NNCI), which was supported by the National Science Foundation (Grant NNCI-2025233). SAXS experiments were performed at the DuPont-Northwestern-Dow Collaborative Access Team (DND-CAT) located at Sector 5 of the Advanced Photon Source (APS). DND-CAT was supported by Northwestern University, The Dow Chemical Company, and DuPond de Nemours, Inc. This research used resources of the Advanced Photon Source, a U.S. Department of Energy (DOE) Office of Science User Facility operated for the DOE Office of Science by Argonne National Laboratory under Contract No. DE-AC02-06CH11357. Data were collected using an instrument funded by the NSF under award number 096 0140. Lab source SAXS experiments were carried out at the University of Minnesota Characterization Facility which receives partial support from the NSF through the MRSEC (award number DMR-2011401) and the NNCI (award number ECCS-2025124) programs. The authors thank the Anton Paar VIP program for the rheometer used in this work. The authors would also like to thank Dr. Stephen I. Pelton and Dr. Vishakha Sabharwal at Boston Medical Center and Boston University for supplying the nontypeable Haemophilus influenzae strain and for their helpful suggestions regarding the chinchilla otitis media model and Steven Weigand, a beamline scientist at DND-CAT, for his help with beamline operations.

Conflict of Interest

S.S.L., J.M.W., F.S.B., M.A.C., and R.Y. are listed as coinventors on a provisional patent (US 63465465), which may include the discoveries reported in this manuscript. All other authors declare no competing interest.

Data Availability Statement

The data that support the findings of this study are available from the corresponding author upon reasonable request.

Keywords

drug delivery, hydrogels, methyl laurate, Otitis media, permeation enhancers

Received: February 5, 2024
Revised: May 8, 2024
Published online:

[1] a) P. Karande, A. Jain, K. Ergun, V. Kispersky, S. Mitragotri, *Proc. Natl. Acad. Sci. USA* **2005**, *102*, 4688; b) Q. D. Pham, S. Bjorklund, J. Engblom, D. Topgaard, E. Sparr, *J. Controlled Release* **2016**, *232*, 175; c) N. Hassan, A. Ahad, M. Ali, J. Ali, *Expert Opin. Drug Delivery* **2010**, *7*, 97; d) S. Maher, D. J. Brayden, *Adv. Drug Delivery Rev.* **2021**, *177*, 113925.

[2] a) A. C. Williams, B. W. Barry, *Adv. Drug Delivery Rev.* **2004**, *56*, 603; b) K. Whitehead, S. Mitragotri, *Pharm. Res.* **2008**, *25*, 1412.

[3] a) S. H. Moghadam, E. Saliaj, S. D. Wettig, C. Dong, M. V. Ivanova, J. T. Huzil, M. Foldvari, *Mol. Pharmaceutics* **2013**, *10*, 2248; b) T. Haque, M. M. U. Talukder, *Adv. Pharm. Bull.* **2018**, *8*, 169.

[4] a) R. Ivanova, P. Alexandridis, B. Lindman, *Colloids Surf., A* **2001**, *183*, 41; b) K. Zhang, B. Lindman, L. Coppola, *Langmuir* **1995**, *11*, 538; c) E. Hecht, K. Mortensen, M. Gradzielski, H. Hoffmann, *J. Phys. Chem.* **1995**, *99*, 4866; d) B. Bharatiya, G. Ghosh, P. Bahadur, J. Mata, *J. Dispersion Sci. Technol.* **2008**, *29*, 696.

[5] a) S. I. Abd-El Hafeez, N. E. Eleraky, E. Hafez, S. A. Abouelmagd, *Sci. Rep.* **2022**, *12*, 5737; b) H. Li, W. Wu, X. Hao, S. Wang, M. You, X. Han, Q. Zhao, B. Xing, *Environ. Pollut.* **2018**, *243*, 206.

[6] a) S. M. A. Ahsan, M. R. Amin, S. Mahbub, M. R. Molla, S. Aktar, M. A. Rub, M. A. Hoque, M. N. Arshad, M. A. Khan, *Chin. J. Chem. Eng.* **2020**, *28*, 216; b) T. S. Banipal, R. Kaur, P. K. Banipal, *J. Mol. Liq.* **2018**, *255*, 113; c) A. M. Khan, S. S. Shah, *J. Dispersion Sci. Technol.* **2009**, *30*, 1247.

[7] R. Yang, V. Sabharwal, O. S. Okonkwo, N. Shlykova, R. Tong, L. Y. Lin, W. Wang, S. Guo, J. J. Rosowski, S. I. Pelton, D. S. Kohane, *Sci. Transl. Med.* **2016**, *8*, 356ra120.

[8] a) J. P. Thomas, R. Berner, T. Zahnert, S. Dazert, *Dtsch. Arztebl. Int.* **2014**, *111*, 151; b) R. Mittal, J. M. Parrish, M. Soni, J. Mittal, K. Mathee, *J. Med. Microbiol.* **2018**, *67*, 1417.

[9] S. W. Hum, K. J. Shaikh, S. S. Musa, N. Shaikh, *J. Pediatr.* **2019**, *215*, 139.

[10] a) M. Axelsson, *BMC Psychol.* **2013**, *1*, 24; b) B. Zielnik-Jurkiewicz, A. Bielicka, *Int. J. Pediatr. Otorhinolaryngol.* **2015**, *79*, 2129; c) R. M. Anderson, *Nat. Med.* **1999**, *5*, 147.

[11] a) G. K. Menon, G. W. Cleary, M. E. Lane, *Int. J. Pharm.* **2012**, *435*, 3; b) G. Volandri, F. Di Puccio, P. Forte, C. Carmignani, *J. Biomech.* **2011**, *44*, 1219; c) L. C. Kuypers, W. F. Decraemer, J. J. Dirckx, *Otol. Neurotol.* **2006**, *27*, 256; d) X. Liu, M. Li, H. Smyth, F. Zhang, *Drug Dev. Ind. Pharm.* **2018**, *44*, 1395.

[12] a) P. S. Roland, M. Wall, *Expert Opin. Pharmacother.* **2008**, *9*, 3129; b) FDA, *Ciprodex: Highlights of prescribing information*, https://www.accessdata.fda.gov/drugsatfda_docs/label/2019/021537s017lbl.pdf (accessed: December 2023).

[13] FDA, *Cetraxal: Highlights of prescribing information*, https://www.accessdata.fda.gov/drugsatfda_docs/label/2009/021918lbl.pdf (accessed: December 2023).

[14] a) X. Khoo, E. J. Simons, H. H. Chiang, J. M. Hickey, V. Sabharwal, S. I. Pelton, J. J. Rosowski, R. Langer, D. S. Kohane, *Biomaterials* **2013**, *34*, 1281; b) R. Yang, O. S. Okonkwo, D. Zurakowski, D. S. Kohane, *J. Controlled Release* **2018**, *289*, 94.

[15] P. Karande, A. Jain, S. Mitragotri, *J. Controlled Release* **2006**, *115*, 85.

[16] a) J. M. White, M. A. Calabrese, *Colloids Surf. A* **2022**, *638*, e128246; b) E. Ruel-Gariepy, J. C. Leroux, *Eur. J. Pharm. Biopharm.* **2004**, *58*, 409; c) K. Mortensen, W. Brown, *Macromolecules* **1993**, *26*, 4128; d) G. Wanka, H. Hoffmann, W. Ulbricht, *Macromolecules* **1994**, *27*, 4145; e) P. Parekh, J. Dey, S. Kumar, S. Nath, R. Ganguly, V. K. Aswal, P. Bahadur, *Colloids Surf., B* **2014**, *114*, 386; f) R. Basak, R. Bandyopadhyay, *Langmuir* **2013**, *29*, 4350; g) P. Alexandridis, V. Athanassiou, S. Fukuda, T. A. Hatton, *Langmuir* **1994**, *10*, 2604.

[17] a) A. Cabana, A. Ait-Kadi, J. Juhasz, *J. Colloid Interface Sci.* **1997**, *190*, 307; b) P. Alexandridis, T. A. Hatton, *Physicochem. Eng. Aspects* **1995**, *96*, 1.

[18] a) B. Z. Chowdhry, M. J. Snowden, S. A. Leharne, *Eur. Polym. J.* **1999**, *35*, 273; b) F. Artzner, S. Geiger, A. Olivier, C. Allais, S. Finet, F. Agnely, *Langmuir* **2007**, *23*, 5085; c) A. E. Beezer, W. Loh, J. C. Mitchell, P. G. Royall, D. O. Smith, M. S. Tute, J. K. Armstrong, B. Z. Chowdhry, S. A. Leharne, *Langmuir* **1994**, *10*, 4001.
[19] a) S. Liu, H. Bao, L. Li, *Eur. Polym. J.* **2015**, *71*, 423; b) K. Suman, S. Sourav, Y. M. Joshi, *Phys. Fluids* **2021**, *33*, 073610; c) J. M. White, A. Garza, J. J. Griebler, F. S. Bates, M. A. Calabrese, *Langmuir* **2023**, *39*, 5084.
[20] I. W. Hamley, V. Castelletto, *Prog. Polym. Sci.* **2004**, *29*, 909.
[21] D. Attwood, J. H. Collett, C. J. Tait, *Int. J. Pharm.* **1985**, *26*, 25.
[22] a) Y. Li, R. Xu, D. M. Bloor, J. F. Holzwarth, E. Wyn-Jones, *Langmuir* **2000**, *16*, 10515; b) Y. Li, R. Xu, S. Couderc, M. Bloor, E. Wyn-Jones, J. F. Holzwarth, *Langmuir* **2001**, *17*, 183; c) S. Kancharla, D. Bedrov, M. Tsianou, P. Alexandridis, *J. Colloid Interface Sci.* **2022**, *609*, 456; d) S. Kancharla, N. A. Zoyhofski, L. Bufalini, B. F. Chatelais, P. Alexandridis, *Polymers (Basel)* **2020**, 12; e) E. Hecht, H. Hoffmann, *Langmuir* **1994**, *10*, 86.
[23] Chemical Book, Methyl laurate: CAS DataBase List, https://www.chemicalbook.com/ChemicalProductProperty_EN_CB6274029.htm (accessed: December 2023).
[24] a) PubChem, *Ciprofloxacin (Compound)*, https://pubchem.ncbi.nlm.nih.gov/compound/Ciprofloxacin (accessed: December 2023); b) A. L. Edmunds, *P T* **2017**, *42*, 307.
[25] PubChem, *Ammonium Chloride*, https://pubchem.ncbi.nlm.nih.gov/compound/Ammonium-Chloride (accessed: December 2023).
[26] R. Yang, V. Sabharwal, N. Shlykova, O. S. Okonkwo, S. I. Pelton, D. S. Kohane, *JCI Insight* **2018**, *3*, e123415.
[27] Y. Zhang, S. Inal, C.-Y. Hsia, M. Ferro, M. Ferro, S. Daniel, R. M. Owens, *Adv. Funct. Mater.* **2016**, *2*, 7304.
[28] H. Tang, S. Mitragotri, D. Blankschtein, R. Langer, *J. Pharm. Sci.* **2001**, *90*, 545.
[29] a) B. Alberts, A. Johnson, J. Lewis, M. Raff, K. Roberts, P. Walter, *Molecular Biology of the Cell*, Garland Science, NY, USA **2002**. b) T. J. Piggot, A. Pineiro, S. Khalid, *J. Chem. Theory Comput.* **2012**, *8*, 4593.
[30] a) E. N. S. F. Bint, H. Su, H. Y. Liu, Z. A. Manzer, Z. Chao, A. Roy, A. M. Pappa, A. Salleo, R. M. Owens, S. Daniel, *ACS Appl. Biol. Mater.* **2021**, *4*, 7942; b) S. Ghosh, Z. Mohamed, J. H. Shin, E. N. S. F. Bint, K. Bali, T. Dorr, R. M. Owens, A. Salleo, S. Daniel, *Biosens. Bioelectron.* **2022**, *204*, 114045.
[31] T. Tang, A. Savva, W. C. Traberg, C. Xu, Q. Thiburce, H.-Y. Liu, A.-M. Pappa, E. Martinelli, A. Withers, M. Cornelius, A. Salleo, R. M. Owens, S. Daniel, *ACS Nano* **2021**, *15*, 18142.
[32] V. Sabharwal, M. Figueira, S. I. Pelton, M. M. Pettigrew, *Microb. Infect.* **2012**, *14*, 712.
[33] a) W. T. Gibson, M. R. Teall, *Food Chem. Toxicol.* **1983**, *21*, 587; b) I. Nicander, S. Ollmar, B. L. Rozell, A. Eek, L. Emtestam, *Br. J. Dermatol.* **1995**, *132*, 718.
[34] FDA, *Otiprio: Highlights of prescribing information*, https://www.accessdata.fda.gov/drugsatfda_docs/label/2018/207986s002lbl.pdf (accessed: November 2023).
[35] a) DailyMed, *Drug label information: Fentanyl system – fentanyl patch*, https://dailymed.nlm.nih.gov/dailymed/drugInfo.cfm?setid=242759ef-cb6d-4e3e-9f8d-5e31efa1f289 (accessed: November 2023); b) DailyMed, *Drug label information: Androderm – testosterone patch*, https://dailymed.nlm.nih.gov/dailymed/drugInfo.cfm?setid=e58a5328-fdd9-40cb-a19f-8ed798989b9c (accessed: November 2023).
[36] a) M. Perez-Vazquez, F. Roman, B. Aracil, R. Canton, J. Campos, *Antimicrob. Agents Chemother.* **2003**, *47*, 3539; b) Y. Hirakata, K. Ohmori, M. Mikuriya, T. Saika, K. Matsuzaki, M. Hasegawa, M. Hatta, N. Yamamoto, H. Kunishima, H. Yano, M. Kitagawa, K. Arai, K. Kawakami, I. Kobayashi, R. N. Jones, S. Kohno, K. Yamaguchi, M. Kaku, *Antimicrob. Agents Chemother.* **2009**, *53*, 4225.
[37] a) K. P. Ananthapadmanabhan, K. Yu, C. L. Meyers, M. P. Aronson, *J. Soc. Cosmet. Chem.* **1996**, *47*, 185; b) S. A. V. Morris, K. P. Ananthapadmanabhan, G. B. Kasting, *J. Pharm. Sci.* **2019**, *108*, 3640.
[38] a) E. A. Mair, A. H. Park, D. Don, J. Koempel, M. Bear, C. LeBel, *JAMA Otolaryngol.–Head Neck Surg.* **2016**, *142*, 444; b) A. H. Park, D. R. White, J. R. Moss, M. Bear, C. LeBel, *Otolaryngol.–Head Neck Surg.* **2016**, *155*, 324.
[39] A. G. M. Schilder, T. Chonmaitree, A. W. Cripps, R. M. Rosenfeld, M. L. Casselbrant, M. P. Haggard, R. P. Venekamp, *Nat. Rev. Dis. Primers* **2016**, *2*, 16063.
[40] a) M. Furtado, L. Chen, Z. Chen, A. Chen, W. Cui, *Eng. Regener.* **2022**, *3*, 217; b) N. Hakuba, Y. Tabata, N. Hato, T. Fujiwara, K. Gyo, *Otol. Neurotol.* **2014**, *35*, 540; c) A. H. Park, C. W. Hughes, A. Jackson, L. Hunter, L. McGill, S. E. Simonsen, S. C. Alder, X. Z. Shu, G. D. Prestwich, *Otolaryngol.–Head Neck Surg.* **2006**, *135*, 877; d) Y. Wang, F. Wen, X. Yao, L. Zeng, J. Wu, Q. He, H. Li, L. Fang, *Front. Bioeng. Biotechnol.* **2021**, *9*, 811652.
[41] L. Kumar, A. Amin, A. K. Bansal, *Pharm. Technol.* **2008**, *32*, 128.
[42] P. A. Heiney, *Int. Union Crystallogr.* **2005**, *32*, 9.
[43] J. C. Phillips, D. J. Hardy, J. D. C. Maia, J. E. Stone, J. V. Ribeiro, R. C. Bernardi, R. Buch, G. Fiorin, J. Hénin, W. Jiang, R. McGreevy, M. C. R. Melo, B. K. Radak, R. D. Skeel, A. Singharoy, Y. Wang, B. Roux, A. Aksimentiev, Z. Luthey-Schulten, L. V. Kalé, K. Schulten, C. Chipot, E. Tajkhorshid, *J. Chem. Phys.* **2020**, *153*, 044130.
[44] A. D. MacKerell Jr., D. Bashford, M. Bellott, R. L. Dunbrack Jr., J. D. Evanseck, M. J. Field, S. Fischer, J. Gao, H. Guo, S. Ha, D. Joseph-McCarthy, L. Kuchnir, K. Kuczera, F. T. K. Lau, C. Mattos, S. Michnick, T. Ngo, D. T. Nguyen, B. Prodhom, W. E. Reiher, B. Roux, M. Schlenkrich, J. C. Smith, R. Stote, J. Straub, M. Watanabe, J. Wiórkiewicz-Kuczera, D. Yin, M. Karplus, *J. Phys. Chem. B* **1998**, *102*, 3586.
[45] J. Huang, A. D. MacKerell Jr, *J. Comput. Chem.* **2013**, *34*, 2135.
[46] a) J. Lee, X. Cheng, J. M. Swails, M. S. Yeom, P. K. Eastman, J. A. Lemkul, S. Wei, J. Buckner, J. C. Jeong, Y. Qi, S. Jo, V. S. Pande, D. A. Case, C. L. Brooks III, A. D. MacKerell Jr., J. B. Klauda, W. Im, *J. Chem. Theory Comput.* **2016**, *12*, 405; b) Y. K. Choi, S.-J. Park, S. Park, S. Kim, N. R. Kern, J. Lee, W. Im, *J. Chem. Theory Comput.* **2021**, *17*, 2431.
[47] W. Humphrey, A. Dalke, K. Schulten, *J. Mol. Graphics* **1996**, *14*, 33.
[48] N. M. O'Boyle, M. Banck, C. A. James, C. Morley, T. Vandermeersch, G. R. Hutchison, *J. Cheminform.* **2011**, *3*, 33.
[49] C. Bannwarth, S. Ehlert, S. Grimme, *J. Chem. Theory Comput.* **2019**, *15*, 1652.
[50] C. Bannwarth, E. Caldeweyher, S. Ehlert, A. Hansen, P. Pracht, J. Seibert, S. Spicher, S. Grimme, *WIREs Comput. Mol. Sci.* **2021**, *11*, e1493.
[51] P. Pracht, F. Bohle, S. Grimme, *Phys. Chem. Chem. Phys.* **2020**, *22*, 7169.
[52] F. Neese, *WIREs Comput. Mol. Sci.* **2022**, *12*, e1606.
[53] a) Y.-S. Lin, G.-D. Li, S.-P. Mao, J.-D. Chai, *J. Chem. Theory Comput.* **2013**, *9*, 263; b) S. Grimme, J. Antony, S. Ehrlich, H. Krieg, *J. Chem. Phys.* **2010**, *132*, 154104.
[54] F. Weigend, R. Ahlrichs, *Phys. Chem. Chem. Phys.* **2005**, *7*, 3297.
[55] R. A. Boto, F. Peccati, R. Laplaza, C. Quan, A. Carbone, J.-P. Piquemal, Y. Maday, J. Contreras-Garcıá, *J. Chem. Theory Comput.* **2020**, *16*, 4150.
[56] Q. Thiburce, N. Melosh, A. Salleo, *Flex. Print. Electron.* **2022**, *7*, 034001.
[57] J. Schindelin, I. Arganda-Carreras, E. Frise, V. Kaynig, M. Longair, T. Pietzsch, S. Preibisch, C. Rueden, S. Saalfeld, B. Schmid, J. Y. Tinevez, D. J. White, V. Hartenstein, K. Eliceiri, P. Tomancak, A. Cardona, *Nat. Methods* **2012**, *9*, 676.